Longitudinal photoelectron momentum shifts induced by absorbing a single XUV photon in diatomic molecules

Di Lao, Pei-Lun He, and Feng He

Longitudinal photoelectron momentum shifts induced by absorbing a single XUV photon in diatomic molecules

Di Lao, Pei-Lun He,* and Feng He†

Key Laboratory for Laser Plasmas (Ministry of Education) and Department of Physics and Astronomy,
Collaborative Innovation Center of IFSA (CICIFSA),
Shanghai Jiao Tong University, Shanghai 200240, China

The photoelectron momentum shifts along the laser propagation are investigated by the time-dependent perturbation theory for diatomic molecules, such as H_2^+, N_2 and O_2. Such longitudinal momentum shifts characterize the photon momentum sharing in atoms and molecules, and oscillate with respect to photon energies, presenting the double-slit interference structure. The atomic and molecular contributions are disentangled analytically, which gives intuitive picture how the double-slit interference structure is formed. Calculation results show the longitudinal photoelectron momentum distribution depends on the internuclear distance, molecular orientation and photon energy. The current laser technology is ready to approve these theoretical predictions.

I.   INTRODUCTION

The rapid development of laser technology has enabled the discovery of many novel phenomena appearing in laser atoms/molecules interactions, among which ionization is one of the most fundamental processes [1]. Many ultrafast measurements are based on ionization and subsequently induced processes [2]. In ionization, photon energies, as well as photon momenta are absorbed by molecular or atomic systems from laser fields.

The concept about ionization has been developed from Einstein's photoelectric effect, to multiphoton ionization, above threshold ionization, and tunneling ionization [3]. In all these processes, photoelectrons carry photon energies, and gain momenta mainly in the laser polarization plane. In these studies, the dipole approximation are widely accepted when a Ti:Sapphire laser pulse with an intensity below 10^{16} W/cm² is introduced [4]. Within the dipole approximation, the photoelectron momentum distribution along the laser propagation direction has a symmetrical distribution centered at zero (see Ref [5–7] for example).

However, due to the small magnitude of a laser wave vector $\mathbf{k}$, the transferred momentum is obscured. This situation justifies the widely adopted dipole approximation in atomic physics, where $|\mathbf{k}|$ is set to be zero. Due to the fact that the dipole approximation is expected to work well when the wavelength of the laser is much longer than the target size, almost all previous investigations beyond the dipole approximation were using short wavelengths and focused on nondipole asymmetry [8–14]. In those topics beyond the dipole approximation [15–20], the law of transferred momentum is one of the most interesting and important topics to study [21–27]. Also, the

transferred momentum due to photo-ionization processes is interpreted as a significant part of radiation pressure, which is of astronomer's interest [28].

It was only very recently that the partition of absorbed photon momenta between nuclei and electrons has been addressed [21]. It was found [25] that for circularly polarized laser pulse in the tunnelling regime, the law of partition is $\langle p_z^e \rangle = \frac{\langle E_k \rangle}{c} + \frac{0.3 I_p}{c}$, $\langle p_z^i \rangle = \frac{0.7 I_p}{c}$, where E_k is the photoelectron energy, I_p is the ionization potential, c is the light speed, $\langle p_z^{e,i} \rangle$ is the expectation value of longitudinal electron or ion momentum. For a linearly polarized light, situations are complex due to the coulomb interaction between nuclei and recoiled electrons [23, 24]. While in the single photon limit, the transferred momentum of electrons and nuclei can be expressed as $\langle p_z^e \rangle = \frac{8}{5}\frac{E_k}{c}$, $\langle p_z^i \rangle = \frac{8}{5}\frac{I_p}{c} - \frac{3}{5}\frac{\omega}{c}$ when the electron is initially in the 1s state [25].

Energy sharing between electrons and nuclei has been studied in the laser-molecule interactions [29–31], while momentum sharing has not been addressed in molecules. In this paper, we studied the longitudinal photoelectron momentum in diatomic molecules in the single photon ionization regime by the time-dependent perturbation theory. A double-slit interference pattern [32–34]for the longitudinal photoelectron momentum distribution is reported, and the interference patterns in H_2^+, N_2 and O_2 are compared and analyzed in details. The rest of this paper is organized as following. In Sec.II we introduce the numerical models. The calculation results for H_2^+, N_2 and O_2 are presented in Sec. III. We end the paper in Sec. IV with a short conclusion.

II.   NUMERICAL METHODS

The single-photon ionization of H_2^+ in XUV fields can be studied by the time-dependent perturbation theory,

which expresses the transition amplitude as

$$M(\mathbf{p}) = -i \int dt \langle \psi_f(t)|H_I|\psi_0(t)\rangle, \qquad (1)$$

where the initial state $\langle \mathbf{r}|\psi_0(t)\rangle = \psi_0(\mathbf{r})\exp[-iI_p(t-t_0)]$ with t_0 being the starting time of the interaction, the final state is described by a plane wave $\langle \mathbf{r}|\psi_f(t)\rangle = \langle \mathbf{r}|\mathbf{p}(t)\rangle = \exp(i\mathbf{p}\cdot\mathbf{r})\exp[-i\frac{p^2}{2}(t-t_0)]$. The interacting Hamiltonian H_I is

$$H_I = \mathbf{A}(t,z)\cdot\mathbf{p} + \frac{1}{2}\mathbf{A}(t,z)^2 \qquad (2)$$

where $\mathbf{A}(t,z)$ is the laser vector potential. We use atomic units throughout this paper unless indicated otherwise. We consider the laser electric field propagates along $+\hat{z}$ direction, and its polarization axis is in the $x-y$ plane. Thus, the vector potential is

$$\mathbf{A}(t,z) = \frac{A_0}{\sqrt{1+\epsilon^2}}\left[\cos(\omega t - kz)\hat{x} + \epsilon\sin(\omega t - kz)\hat{y}\right], \quad (3)$$

where k is the wave number or the photon momentum. When $\epsilon = 0$ or 1, the laser field is linearly or circularly polarized. For an infinite long laser pulse, the integration in Eq. (1) yields

$$M(\mathbf{p}) \propto \frac{A_0}{\sqrt{1+\epsilon^2}}(p_x + i\varepsilon p_y)\langle \mathbf{p} - k\hat{z}|\psi_0\rangle\delta(\omega - p^2/2 - I_p). (4)$$

The $\delta(\omega - p^2/2 - I_p)$ guarantees the energy conservation. Finally, the expectation value of the photoelectron momentum p_z can be calculated via

$$\langle p_z\rangle = \frac{\oint_S d^3\mathbf{p}\, p_z(p_x^2 + \varepsilon^2 p_y^2)|\langle \mathbf{p} - k\hat{z}|\psi_0\rangle|^2}{\oint_S d^3\mathbf{p}\,(p_x^2 + \varepsilon^2 p_y^2)|\langle \mathbf{p} - k\hat{z}|\psi_0\rangle|^2}, \qquad (5)$$

where S represents the integral surface satisfying $\frac{1}{2}p^2 = \omega - I_p$. $|\langle \mathbf{p} - k\hat{z}|\psi_0\rangle|^2$ is the initial momentum probability distribution for the bound electron after shifting $k\hat{z}$.

For H_2^+, the molecular orbitals can be roughly constructed by combining the two atomic states, i.e.,

$$\psi_{g/u}(\mathbf{r}) = \psi_{atom}(\mathbf{r} - \mathbf{R}/2) \pm \psi_{atom}(\mathbf{r} + \mathbf{R}/2), \quad (6)$$

where $|\mathbf{R}|$ is the internuclear distance and ψ_{atom} is the atomic state. The corresponding molecular wavefunction in momentum representation is

$$|\psi_g(\mathbf{p})|^2 = |\psi_{atom}(\mathbf{p})|^2\cos^2(\mathbf{p}\cdot\mathbf{R}/2),$$
$$|\psi_u(\mathbf{p})|^2 = |\psi_{atom}(\mathbf{p})|^2\sin^2(\mathbf{p}\cdot\mathbf{R}/2). \qquad (7)$$

Insertion of Eq. (7) into Eq. (5) yields the the expectation value of p_z,

$$\langle p_z\rangle = \langle p_z\rangle_{atom} + \langle p_z\rangle_{osc}, \qquad (8)$$

which are contributed by the atoms and the interference of two centers, respectively. The conclusion indicated by Eq. (8) was deduced from H_2^+, but it should work for
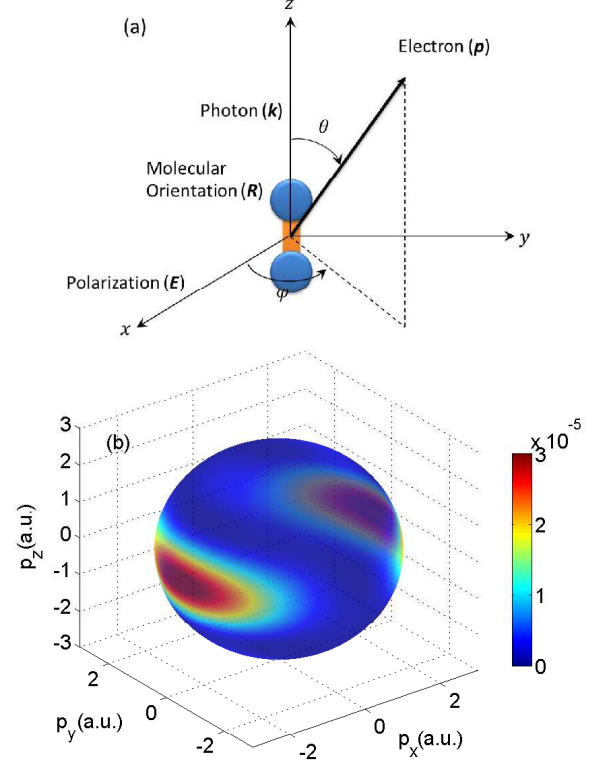

FIG. 1: (a) Geometry applicable to a linearly polarized field with H_2^+ aligned along z axis. (b) The photoelectron momentum angular distribution of H_2^+ with internuclear distance $R = 2$ and photon energy $\omega = 4.5$ a.u..

general diatomic molecules. For more complex diatomic molecules, such as N_2 and O_2, we calculate the molecular orbitals by using the MOLPRO [35]. In later calculations for N_2 and O_2, we set the bond lengths at $R_{N_2} = 2.07\,a.u.$ and $R_{O_2} = 2.2\,a.u.$, respectively. In MOLPRO, we used the Gaussian type orbital (GTO) basis cc-pVTZ and calculated the coefficients and exponents for different GTO basis, with which the molecular orbitals are constructed.

III. CALCULATION RESULTS

For atoms initially in different states, the transferred longitudinal momenta from photon momenta are different [36]. For molecules, we expect the longitudinal momenta are more complex due to multi-coulombic centers. For H_2^+ at $R = 2$ a.u., we set $\lambda = 1.236$ and the molecular wavefunction is written as

$$\psi_0(\mathbf{r}) = \frac{\lambda^{3/2}}{\sqrt{\pi}}(e^{-\lambda|\mathbf{r}-\frac{1}{2}\mathbf{R}|} + e^{-\lambda|\mathbf{r}+\frac{1}{2}\mathbf{R}|}). \qquad (9)$$

The laser-molecule interaction geometry is sketched in Fig. 1 (a). The XUV field propagates along $+z$ axis, and its polarization axis is in the $x-y$ plane. The photoelec-

tron momentum angular distribution is sketched in Fig. 1 (b).

Within the dipole approximation, the photoelectron only gains momenta in the laser polarization plane from the laser field. The momentum distribution along the laser propagation axis is symmetrical with respect to $p_z = 0$. Therefore the expectation value of longitudinal momentum $\langle p_z \rangle$ should be 0. In the laser polarization plane, the Coulomb potential drags the photoelectron when it escapes from the parent ion, and gives rise to a tilt angle for the photoelectron angular distribution [37]. Though the Coulomb potential modifies the photoelectron distribution, it does not change the fine structures. Especially, when the electron escapes from the nucleus very quickly, the Coulomb action can be neglected. In the following calculations, we use very high-energetic photons, thus the Coulomb potential can be safely neglected. It has also been shown in Ref [25] that the distribution of p_z and $\langle p_z \rangle$ are not affected by the Coulomb corrections when the electron is initially in 1s atomic state.

After introducing the nondipole effect, the center of the longitudinal momentum is shifted away from $p_z = 0$ to $p_z = k$. According to Eq. (8), $\langle p_z \rangle$ of diatomic molecules may present more complex structures beyond the shift which happens in atoms. For H_2^+, when the electron is kicked by the photon along $+z$ axis, the electron may fly away from both nuclei, thus $\langle p_z \rangle$ component may show some interference patterns. To numerically prove that, we insert Eq. (9) into Eq. (5) and obtain

$$\langle p_z \rangle = \frac{\int_S d^3\mathbf{p}\, p_z (p_x^2 + p_y^2) \frac{1}{(\lambda^2 + (\mathbf{p} - k\hat{z})^2)^4} \cos^2[\frac{\mathbf{R}}{2} \cdot (\mathbf{p} - k\hat{z})]}{\int_S d^3\mathbf{p}\, (p_x^2 + p_y^2) \frac{1}{(\lambda^2 + (\mathbf{p} - k\hat{z})^2)^4} \cos^2[\frac{\mathbf{R}}{2} \cdot (\mathbf{p} - k\hat{z})]},$$

(10)

The cosine term in the integration in Eq. (10) carries the double-slit interference, which should depend on both the molecular orientation and internuclear distance.

Fig. 2 (a) shows the expectation value of longitudinal momentum $\langle p_z \rangle$ as a function of the photoelectron energy. The black dash-dotted curve and the brown dashed curve are for H_2^+ aligned along x axis and y axis, respectively, and the XUV field is linearly polarized along the x axis. The red solid curve is for the case that H_2^+ is aligned along x axis and the XUV field is circularly polarized in $x - y$ plane. The dotted horizontal line indicates $\langle p_z \rangle$ for a hydrogen atom in the ground state. It is clear that $\langle p_z \rangle$ oscillates around the equilibrium position $\langle p_z \rangle = 1.6E_k/c$. The oscillation amplitude gradually decays with the increasing of the photoelectron energy. And the oscillation amplitude depends on the orientations of molecule. When the molecular axis and the laser polarization axis are parallel to each other, the oscillation amplitude is larger than that when these two directions are orthogonal to each other. When the laser field is circularly polarized, the oscillated $\langle p_z \rangle$ is similar to the case using linearly polarized laser pulse after averaging over
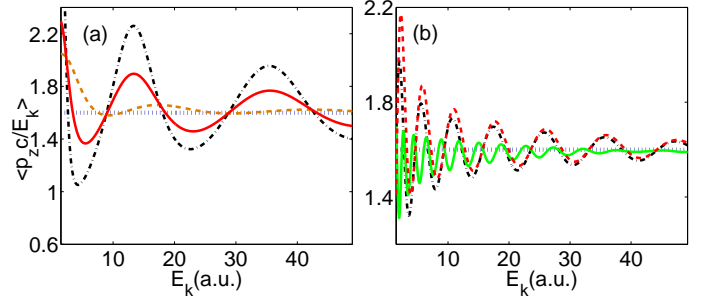

FIG. 2: (a) The expectation value of the longitudinal photoelectron momentum as a function of the photoelectron kinetic energy. The blue dotted line represents the result for a hydrogen atom, and the black dash-dotted line, brown dashed line, red solid line are the results for H_2^+ aligned along x axis with a linearly polarized laser pulse, aligned along y axis with a linearly polarized laser pulse, and aligned along x axis with a circularly polarized laser pulse. The internuclear distance is 2 a.u.. (b) The expectation value of longitudinal photoelectron momentum with respect to the photoelectron energy for $R = 5$ (black dash-dotted line) and $R = 10$ (green solid line) is shown. The blue dotted line is same as that in (a). The red dashed line is the analytical result governed by Eq. (11). The circularly polarized XUV field is implemented.

all molecular orientations. The oscillation of $\langle p_z \rangle$ also depends on the internuclear distance, as shown in Fig. 2 (b). For a larger internuclear distance, the separation between neighboring peaks is smaller, which is consistent to the general double-slit interference pattern.

The fluctuation of $\langle p_z \rangle$ can be viewed in an analytical form. In the high-photon-energy limit, $\frac{1}{(\lambda^2 + p^2 + k^2 - 2kp\cos\theta)^4}$ in Eq. (10) can be further expanded as $\frac{1}{(\lambda^2 + p^2 + k^2)^4}(1 + \frac{8kp\cos\theta}{\lambda^2 + p^2 + k^2})$ by discarding high-order terms. With this, when the molecular axis is parallel to the laser propagation axis, Eq. (10) can be analytically written as

$$\langle p_z \rangle = \frac{8}{5}\frac{E_k}{c}\left[1 - \frac{6}{R^2 E_k}\cos\alpha\cos\beta - \frac{15c}{8\sqrt{2}R^2 E_k^{3/2}}\sin\alpha\sin\beta\right],$$

(11)

where $\alpha = Rp$, $\beta = Rk$. It is clear that the first term in Eq. (11) is the atomic contribution, and the two latter terms lead to the oscillation of $\langle p_z \rangle$. In high energy limit, the second term is more important than the third term since the third one decays faster. $\cos(\alpha)$ clearly describes the double-slit interference for the photoelectron releasing from two nuclei. $\cos(\beta)$ describes the double-slit interference contributed by the photon momentum. The product of $\cos(\alpha)$ and $\cos(\beta)$ contributes to the main oscillation of $\langle p_z \rangle$ when E_k is large. We plotted $\langle p_z \rangle$ governed by Eq. (11) in Fig. 2 (b) for $R = 5$ a.u. One may clearly see that Eq. (11) matches the simulation results very well especially when E_k is very large.

The double-slit interference showing in $\langle p_z \rangle$ exists not only in the simplest molecule H_2^+, but also in more general diatomic molecules. According to Eq. (5), the ul-
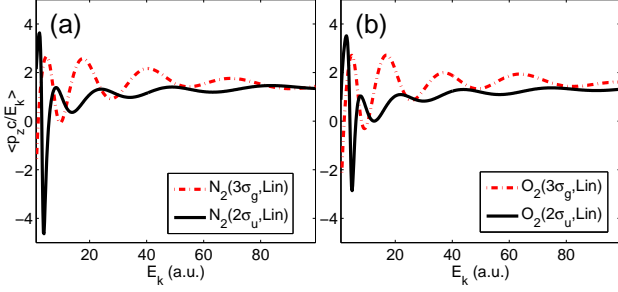
FIG. 3: (a) The expectation value of the longitudinal momentum distribution as a function of E_k for the photoelectron initially in $3\sigma_g$ (red dash-dotted curve) and $2\sigma_u$ (black solid curve) of N_2. The molecule is aligned along z axis, and the XUV filed is linear polarized along x axis. (b) Same as (a) but for O_2. The ionization potentials for $2\sigma_u$ and $3\sigma_g$ of N_2 (O_2) are 0.78 (1.08) and 0.63 (0.745) a.u., respectively.

FIG. 4: (a) The momentum probability distribution in the logarithmic scale for the bound electron in $2\sigma_u$ of N_2 shifted by k along p_z axis. Here, $k = 0.033$ a.u.. (b) The photoelectron momentum angular distribution for the electron initially at $2\sigma_u$ of N_2. $\omega = 4.5$ a.u..

timate $\langle p_z \rangle$ should also depend on initial molecular orbitals. We now study the $\langle p_z \rangle$ of the photoelectron from N_2 and O_2. Figure 3 (a) shows the $\langle p_z \rangle$ as a function of E_k for the photoelectron initially in $3\sigma_g$ (red dash-dotted curve) and $2\sigma_u$ (black solid curve) states. The $3\sigma_g$ orbital is constructed by two symmetrical atomic $2p_z$ states, and the $2\sigma_u$ orbital is constructed by two asymmetrical atomic $2s$ states. We only consider the response of a single electron in the XUV fields though electrons in the inner orbital might have larger cross section to be ionized. This assumption will capture some phenomena qualitatively and work as a prototype. The double-slit interference pattern is still observed. This oscillated $\langle p_z \rangle$ finally converges to atomic case with the increasing of E_k. The similar behavior are preserved for O_2, as shown in Fig. 3 (b). In both panels, the phases of the oscillated $\langle p_z \rangle$ from $2\sigma_u$ and $3\sigma_g$ are opposite, which is due to the opposite phase for these two orbitals.

When E_k is relatively small, $\langle p_z \rangle$ could be negative though the laser propagates along $+z$ axis. And as a matter of fact, this can be understood by looking into the atomic states. For $2\sigma_u$ of N_2, which is constructed by two asymmetrical atomic $2s$ states, the transferred longitudinal momenta are governed by the formula $\frac{8}{5}\frac{E_k}{c}(1 - \frac{1}{E_k})$ [36]. Viewing from this formula, negative value of $\langle p_z \rangle$ occurs when E_k is small. Alternatively, the negative value of $\langle p_z \rangle$ can be understood by looking into Eq. (5), which shows that the photoelectron momentum distribution is proportional to $|\langle \mathbf{p} - k\hat{z}|\psi_0 \rangle|^2$. Fig. 4(a) shows $|\langle \mathbf{p} - k\hat{z}|\psi_0 \rangle|^2$ for $2\sigma_u$ of N_2. The sketched molecular orbital in space coordinates is shown in the right-bottom corner. The p_z distribution can be factorized as the atomic momentum distribution shifted by k, and a series of subpeaks determined by a structure factor $\sin^2[(p_z - k)R/2]$. The whole picture should be symmetrical with respect to $p_z = k$ and asymmetrical with respect to $p_z = 0$. However, k is usually very small, for example, $k = 0.033$ a.u. in the case that $\omega = 4.5$ a.u.,
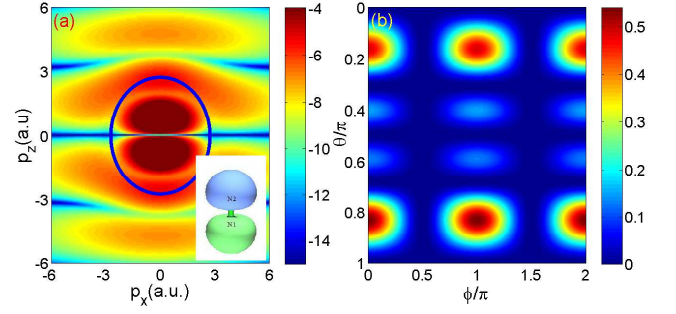
thus the asymmetry in Fig. 4 (a) is hardly visible. According to Eq. 4, $\delta(\omega - p^2/2 - I_p)$ manifests itself as a ring satisfying $p_x^2 + p_z^2 = 2(\omega - I_p)$ in the plane $p_y = 0$, as shown by the circle in Fig. 4 (a) [38]. The non-negligible k results in the upward shift of the electron momentum distribution, which moves subpeaks in Fig. 4 (a) either closer or further to the circle, depending on its radius. The $\langle p_z \rangle$ depends on the subpeak which is closest to the circle. In the case that $\omega = 4.5$ a.u., the subpeak in the lower half space in Fig. 4 (a) moves closer to the circle, thus the photoelectron with $p_z < 0$, shown in Fig. 4(b), has a larger probability than that of $p_z > 0$. The asymmetrical distributions in the upper and lower half spaces make the averaged $\langle p_z \rangle < 0$. For a different photon energy ω, the upshifted subpeaks in the upper half space in Fig. 4 (a) might move closer to the circle, resulting in $\langle p_z \rangle > 0$. Therefore, $\langle p_z \rangle$ oscillates with respect to ω or E_k. Of course, in the dipole approximation, $\langle p_z \rangle$ is always zero because the small k is neglected, and thus the symmetrical distribution with respect to $p_z = 0$ is always preserved.

Before ending this section, we may point that Hosaka et al. [39] and Toffoli et al. [40] discussed the interference induced by the nondipole effect in the N_2 molecule, and this interference was further explained by the orbital-dependent nondipole angular parameters.

IV. CONCLUSIONS

In conclusion, by including the photon momentum transferred into the atom beyond the dipole approximation, the expectation value of longitudinal photoelectron momentum $\langle p_z \rangle$ shifts away from zero. In diatomic molecules, $\langle p_z \rangle$ oscillates with respect to the photon energy. Two factors contribute to such oscillation: the double-slit interference of the photoelectron $\cos(\alpha)$ and the double-slit interference of the photon $\cos(\beta)$. As shown above, the interference pattern occurs in all diatomic molecules. The present work indicates the im-

portance of the photon momentum sharing in photoionization. The fruitful structures of $\langle p_z \rangle$ offers another perspective to extract molecular information.

[1] T. Brabec and F. Krausz, "Intense few-cycle laser fields: Frontiers of nonlinear optics", Rev. Mod. Phys. **72**, 545 (2000).

[2] F. Krausz and M. Ivanov, "Attosecond physics", Rev. Mod. Phys. **81**, 163 (2009).

[3] W. Becker, F. Grasbon, R. Kopold, D. B. Milošević, G. G. Paulus and H. Walther, "Above-threshold ionizaiton: from classical features to quantum effects", Advances in atomic, molecular and optical physics **48**, 35 (2002).

[4] M. Førre, J. P. Hansen, L. Kocbach, S. Selstø and L. B. Madsen, "Nondipole Ionization Dynamics of Atoms in Superintense High-Frequency Attosecond Pulses", Phys. Rev. Lett. **97**, 043601 (2006).

[5] I. A. Ivanov, "Evolution of the transverse photoelectron-momentum distribution for atomic ionization driven by a laser pulse with varying ellipticity", Phys. Rev. A **90**, 013418 (2014).

[6] I. Petersen, J. Henkel, and M. Lein, "Signatures of molecular orbital structure in lateral electron momentum distributions from strong-field ionization", Phys. Rev. Lett. **114**, 103004 (2015).

[7] L. Arissian, C. Smeenk, F. Turner, C. Trallero, A. V. Sokolov, D. M. Villeneuve, A. Staudte, and P. B. Corkum, "Direct test of laser tunneling with electron momentum imaging", Phys. Rev. Lett. **105**, 133002 (2010).

[8] B. Krässig, M. Jung, D. S. Gemmell, E. P. Kanter, T. LeBrun and S. H. Southworth and L. Young, "Nondipolar Asymmetries of Photoelectron Angular Distributions", Phys. Rev. Lett. **75**, 4736 (1995).

[9] M. Jung, B. Krässig, D. S. Gemmell, E. P. Kanter, T. LeBrun, S. H. Southworth, and L. Young, "Experimental determination of nondipolar angular distribution parameters for photoionization in the Ar K and Kr L shells", Phys. Rev. A **54**, 2127 (1996).

[10] O. Hemmers, H. Wang, P. Focke, I. A. Sellin, D. W. Lindle, J. C. Arce, J. A. Sheehy, and P. W. Langhoff, "Large Nondipole Effects in the Angular Distributions of K-Shell Photoelectrons from Molecular Nitrogen", Phys. Rev. Lett. **87**, 273003 (2001).

[11] S. Ricz, R. Sankari, Á. Kövér, M. Jurvansuu, D. Varga, J. Nikkinen, T. Ricsoka, H. Aksela, and S. Aksela, "Strong nondipole effect created by multielectron correlation in 5s photoionization of xenon", Phys. Rev. Lett. **67**, 012712 (2003).

[12] B. Krässig, J.-C. Bilheux, R. W. Dunford, D. S. Gemmell, S. Hasegawa, E. P. Kanter, S. H. Southworth, L. Young, L. A. LaJohn, and R. H. Pratt, "Nondipole asymmetries of Kr 1s photoelectrons", Phys. Rev. A **67**, 022707 (2003).

[13] O. Hemmers, R. Guillemin, D. Rolles, A. Wolska, D. W. Lindle, E. P. Kanter, B. Krässig, S. H. Southworth, R.Wehlitz, B. Zimmermann, V. McKoy and P. W. Langhoff, "Low-Energy Nondipole Effects in Molecular Nitrogen Valence-Shell Photoionization", Phys. Rev. Lett. **97**, 103006 (2006).

[14] A. N. Grum-Grzhimailo and E.V. Gryzlova, "Nondipole effects in the angular distribution of photoelectrons in two-photon two-color above-threshold atomic ionization", Phys. Rev. A **89**, 043424 (2014).

[15] H. R. Reiss, "Relativistic effects in nonrelativistic ionization", Phys. Rev. A **87**, 033421 (2013).

[16] M. Klaiber, E. Yakaboylu, H. Bauke, K. Z. Hatsagortsyan and C. H. Keitel, "Under-the-Barrier Dynamics in Laser-Induced Relativistic Tunneling", Phys. Rev. Lett. **110**, 153004 (2013).

[17] E. Yakaboylu, M. Klaiber, H. Bauke, K. Z. Hatsagortsyan and C. H. Keitel, "Relativistic features and time delay of laser-induced tunnel ionization", Phys. Rev. A **88**, 063421 (2013).

[18] H. R. Reiss, "Mass shell of strong-field quantum electrodynamics", Phys. Rev. A **89**, 022116 (2014).

[19] I. A. Ivanov, "Relativistic calculation of the electron-momentum shift in tunneling ionization", Phys. Rev. A **91**, 043410 (2015).

[20] S. Chelkowski, A. D. Bandrauk and P. B. Corkum, "Photon-momentum transfer in multiphoton ionization and in time-resolved holography with photoelectrons", Phys. Rev. A **92**, 051401 (2015).

[21] C. T. L. Smeenk, L. Arissian, B. Zhou, A. Mysyrowicz, D. M. Villeneuve, A. Staudte and P. B. Corkum, "Partitioning of the Linear Photon Momentum in Multiphoton Ionization", Phys. Rev. Lett. **106**,193002 (2011).

[22] A. S. Titi and G. W. F. Drake, "Quantum theory of longitudinal momentum transfer in above-threshold ionization", Phys. Rev. A **85**,041404 (2012).

[23] J. Liu, Q. Z. Xia, J. F. Tao and L. B. Fu, "Coulomb effects in photon-momentum partitioning during atomic ionization by intense linearly polarized light", Phys. Rev. A **87**, 041403 (2013).

[24] A. Ludwig, J. Maurer, B. W. Mayer, C. R. Phillips, L. Gallmann and U. Keller, "Breakdown of the Dipole Approximation in Strong-Field Ionization", Phys. Rev. Lett. **113**, 243001 (2014).

[25] S. Chelkowski, A. D. Bandrauk and P. B. Corkum, "Photon Momentum Sharing between an Electron and an Ion in Photoionization: From One-Photon (Photoelectric Effect) to Multiphoton Absorption", Phys. Rev. Lett. **113**, 263005 (2014).

[26] D. Cricchio, E. Fiordilino and K. Z. Hatsagortsyan, "Momentum partition between constituents of exotic atoms during laser-induced tunneling ionization", Phys. Rev. A **92**, 023408 (2015).

[27] K. Krajewska and J. Z. Kamiński, "Radiation pressure in strong-field-approximation theory: Retardation and recoil corrections", Phys. Rev. A **92**, 043419 (2015).

[28] G. Michaud, "Diffusion Processes in Peculiar a Stars", The Astrophysical Journal **160**, 641 (1970).

[29] C. B. Madsen, F. Anis, L. B. Madsen, and B. D. Esry, "Multiphoton Above Threshold Effects in Strong-Field Fragmentation", Phys. Rev. Lett. **109**, 163003 (2012).

[30] J. Wu, M. Kunitski, M. Pitzer, F. Trinter, L. Ph. H. Schmidt, T. Jahnke, M. Magrakvelidze, C. B. Madsen, L. B. Madsen, U. Thumm, and R. Dörner, "Electron-Nuclear Energy Sharing in Above-Threshold Multiphoton Dissociative Ionization of H_2", Phys. Rev. Lett. **111** 023002 (2013).

[31] R. Silva, F. Catoire, P. Riviere, H. Bachau, and F. Martin, "Correlated Electron and Nuclear Dynamics in Strong Field Photoionization of H_2^+", Phys. Rev. Lett. **110**, 113001 (2013).

[32] H. D. Cohen and U. Fano, "Interference in the Photo-Ionization of Molecules", Phys. Rev **150**, 30 (1966).

[33] R. K. Kushawaha, M. Patanen, R. Guillemin, L. Journel, C. Miron, M. Simon, M. N. Piancastelli, C. Skates and P. Decleva, "From double-slit interference to structural information in simple hydrocarbons", PNAS **110**, 15201-15206 (2013).

[34] X. J. Liu, Q. Miao, F. Gel'mukhanov, M. Patanen, O. Travnikova, C. Nicolas, H. Ågren, K. Ueda and C. Miron, "Einstein-Bohr recoiling double-slit gedanken experiment performed at the molecular level", Nature Photonics **9**, 120 (2014).

[35] H. J. Werner et al., MOLPRO, version 2010.1, 2010. See http://www.molpro.net.

[36] M. J. Seaton, "Momentum transfer in photo-ionization processes", J. Phys. B **28**, 3185 (1995).

[37] P. L. He, Norio Takemoto and F. He, "Photoelectron momentum distributions of atomic and molecular systems in strong circularly or elliptically polarized laser fields", Phys. Rev. A **91**, 063413 (2015).

[38] P. L. He and F. He, "Ionization of H_2^+ in XUV pulses", Phys. Scrs **90**, 045402 (2015).

[39] K. Hosaka, J. Adachi, A. V. Golovin, M. Takahashi, T. Teramoto, N. Watanabe, A. Yagishita, S. K. Semenov and N. A. Cherepkov, "Non-dipole effects in the angular distribution of photoelectrons from the K-shell of N_2 molecule", J. Phys. B: At. Mol. Opt. Phys. **39**, L25(2006).

[40] D. Toffoli and P. Decleva, "Photoelectron angular distributions beyond the dipole approximation: a computational study on the N_2 molecule", J. Phys. B: At. Mol. Opt. Phys. **39**, 2681(2006).